LEGIBILITY NOTICE

A major purpose of the Technical Information Center is to provide the broadest dissemination possible of information contained in DOE's Research and Development Reports to business, industry, the academic community, and federal, state and local governments.

Although a small portion of this report is not reproducible, it is being made available to expedite the availability of information on the research discussed herein.

LA-UR -90-1514

CONF-900907--2

Los Alamos National Laboratory is operated by the University of California for the United States Department of Energy under contract W-7405-ENG-36

LA-UR--90-1514

DE90 012100

TITLE MICROSEISMIC MONITORING OF THE CHAVEROO OIL FIELD, NEW MEXICO

AUTHOR(S) James T. Rutledge
James N. Albright
Thomas D. Fairbanks
Mark B. Murphy
Peter M. Roberts

SUBMITTED TO Society of Exploration Geophysicists
1990 Annual Meeting
San Francisco, CA
September 23-27, 1990

DISCLAIMER

Los Alamos Los Alamos National Laboratory
Los Alamos, New Mexico 87545

FORM NO. 836 R4

DISTRIBUTION

MASTER

Microseismic Monitoring of the Chaveroo Oil Field, New Mexico

James T. Rutledge, James N. Albright, Thomas D. Fairbanks, Mark B. Murphy, and Peter M. Roberts

SUMMARY

Induced microseismicity was monitored in the Chaveroo oil field in southeastern New Mexico during a pressurized stimulation of a well being prepared as an injector for a waterflood operation. In addition, the microseismicity was monitored for 5 weeks following the stimulation while the area was under normal waterflood production. Little seismicity was detected during the 5.5 hour stimulation in which three thousand barrels of water were injected into the reservoir at pressures ranging from 96 to 257 bars in excess of hydrostatic pressure. Intermittent monitoring over the 5-week period indicated detectable seismicity occurred during waterflood production. Monitoring during the 5 weeks, however, was not complete enough to draw general conclusions on temporal variations of observed microseismicity. Seventy-three good quality events recorded over a cumulative 24 hours of intermittent monitoring were located using the hodogram technique. Events were detected at distances up to 1700 m from the monitor well but most occurred within 900 m. The map of microearthquake locations indicates that events occurred in the vicinity of producing wells and away from injection wells. The first half of the sequence of mappable events occurred along linear trends, but the pattern became more scattered during the later half of the sequence.

The lack of seismicity during the pressurized injection and the increased seismicity levels occurring away from injection wells during waterflood production, suggest seismicity is not induced by Mohr-Coulomb failure. We suspect, as proposed by previous investigators, that seismicity could be induced by the decrease of pore pressure resulting from reservoir fluid withdrawl.

INTRODUCTION

Oil is produced from the San Andres Formation in several individual fields that extend over an area of more than 100 miles across the Permian basin of west Texas and eastern New Mexico. The Chaveroo oil field in southeastern New Mexico has alone produced 23.1 million barrels of oil. Since 1965, the Chaveroo field has been under primary production and is just beginning to undergo enhanced recovery by waterflooding. One problem with waterflooding in some fields producing from the San Andres Formation is flow anisotropy in the reservoir due to preferred flow along fractures. This can result in premature breakthroughs between injection and producing wells which reduces oil recovery. If the locations of major fractures in the reservoir were known, then waterfloods could be designed with well configurations which would delay breakthroughs and improve recovery. The Chaveroo field has wells spaced uniformly at 400 m in a grid pattern parallel with section boundaries. Pressure interference testing has not been successful due to the large well separation, and the density of wells is insufficient to accurately infer flow direction from breakthrough patterns alone. Microseismic monitoring is an alternative method for determining the location and prevalent orientations of fractures. The method has been successfully used in crystalline rock for mapping hydraulic fractures (e.g. Fehler et al.,1987). The method relies on the observation that microearthquakes occur along fractures that make up flow paths when stress is changed along the fractures by increased fluid pressure. By determining the locations of the induced microearthquakes, some knowledge of the locations and orientations of the dominant fluid paths is obtained. If the method can be shown to be successful in the San Andres Formation, it could be a useful tool for optimizing waterfloods in the Chaveroo field and other fields producing from the San Andres Formation.

The microseismicity of the San Andres Formation in the Chaveroo oil field was monitored during, and for 5 weeks following, a pressurized stimulation of a well being prepared as an injector for a waterflood operation. The objective of the study was to determine if seismicity

was detectable in the San Andres Formation during well stimulation and during normal waterflood production at rates practical for mapping the fractures along which microearthquakes occur.

EXPERIMENTAL SET-UP

The experiment was conducted in Section 34 of the Murphy Operating Corporation's (MOC) Haley Unit of the Chaveroo field (Figure 1). Oil is produced from 3 porosity zones over the depth interval 1265-1330 m in the Chaveroo field. Three thousand barrels of water were pumped into well 34-10 (Figure 1) in the intermediate porosity zone at approximately 1300 m depth. During the pressurized injection, two 3-component borehole geophone packages were placed in wells 34-7 and 34-11 located about 400 m directly north and west, respectively, from the injection well. Both geophone packages were stationed at 1280 m depth, just above the perforated casing of the shallowest porosity zone, putting them close to the expected depth of microseismic activity. An explosive charge was detonated in a shallow hole near well 34-15 for orienting the horizontal components of the geophone tools.

Injection took place on June 7, 1989 and lasted 5.5 hours. The pumping rate was initially 8.0 barrels per minute and was increased in steps up to a maximum of 10.5 barrels per minute by the end of pumping. Pressures ranged from 96 to 257 bars in excess of hydrostatic pressure over the pumping period. After pumping, the geophone package in well 34-11 was removed. The geophone tool in well 34-7 was left in place to continue monitoring the field for a 5-week period ending on July 13. Following the pressurized injection, wells 34-2, 34-4, 34-10 and 34-12 began taking water under hydrostatic pressure at a rate of about 200 to 250 barrels per day and remained on line as injectors throughout the 5 week monitoring period. Pressure at the depth of the injection (approximately 1300 m) was about 130 bars when the wells were full to the surface. Except for well 34-16, the remaining wells of Section 34 went back on line as producers within 5 days following the stimulation of well 34-10.

Seismic data were recorded on analog tape throughout the pressurized injection of June 7 and for several hours thereafter. Monitoring during the 5 following weeks was not continuous. Post-injection data were recorded using both analog tape and a digital event recorder. The digital recorder stored signals captured by an algorithm which triggered on signal levels of a specified amount over a continuously-measured, background level. On the average, the memory of the digital recorder filled in about 40 hours. The total time covered by the digital recorder was 315 hours over the 5 weeks following injection. An additional 76 hours of data were recorded on analog tape during 7 different nights. Night recordings had substantially less noise than daytime recordings.

MICROSEISMIC DATA

The analog field tapes were played back through a computer based, data-acquisition system. Microearthquake signals triggering the system were digitized at a sample interval of 0.2 ms. The data recorded digitally in the field were limited to a minimum sample interval of 2.0 ms. Microearthquakes were defined as signals with clearly defined compressional-wave (P) and shear-wave (S) arrivals. One-hundred-fifty-four events were selected from the analog data and 115 events from the digital data. The time distribution of the event occurrences for the two data sets are shown in Figures 2 and 3. Monitoring was not continuous over the 5 weeks following injection resulting in large gaps in time when data were not gathered. Only 4 events were detected during the 5.5-hour pressurized injection and these events were only detected in well 34-7. The sensitivity of the geophone package in well 34-11 was less, and apparently too small

to detect the few events recorded in well 34-7. The computer algorithm used in digitizing the analog data enabled the detection of more microearthquakes over shorter intervals of time than was possible with the field digital recorder.

Most of the microearthquakes that were observed occurred during the period June 19-23. Since there were gaps in the data acquisition, it is not known when the microearthquake activity in the section actually peaked or how it fluctuated throughout the 5 weeks. The period of maximum seismic activity shows no simple correlation with the production activity of Section 34. Both data sets show decreasing seismic activity from the high of June 19 until July 1 when the field digital recorder showed an increase in activity. The analog data recorded after June 23 is contaminated by high frequency noise of unknown origin, which, because the signal-to-noise ratio of events is lowered, makes triggering the data acquisition system more difficult. The field digital data was not affected by the higher frequency noise because of anti-alias filters.

The three components of particle velocity and a displacement amplitude spectrum of a representative event are shown in Figure 4. In general, the displacement amplitude spectra have a shape similar to shear-slip seismic events. The corner frequencies range between about 50 and 90 Hz. The spectra's frequency roll off above the corner ranges between ω^{-2} and ω^{-3},where ω is angular frequency. This value range is also typical of shear-slip seismic events (Aki and Richards, 1980).

DATA ANALYSIS AND RESULTS

If the velocity structure is accurately known, microearthquake locations can be determined uniquely from P- and S-wave arrival times detected at a minimum of 3 stations. Having only recorded events at one 3-component station, we were limited to mapping using the hodogram technique in which distance is determined from the S-P arrival time difference, and direction to the event is determined from the P-wave particle motion of the first arrival. The direction to the event is taken as the orientation of the major axis of an ellipsoid fitted to the 3-dimensional seismic particle motion of the P-wave (Matsumura, 1981). We have applied the method in 2-dimensions by fitting an ellipse to the horizontal components of particle motion. The vertical component was not used because it contained a strong resonance at higher frequencies than the horizontal components, and its first arrivals had poor signal-to-noise ratios. The degraded signal-to-noise ratio results from consistently smaller P-wave arrivals on the vertical axis, as seen in Figure 4. First arrivals from the orientation shot at the surface have a much stonger P-wave arrival on the vertical component than on the horizontals as would be expected from its steep angle of approach to the geophone. The smaller vertical-component P-wave arrivals for the microearthquakes imply that seismicity is restricted to depths close to the geophone depth, that is, within or near the producing zones of the reservoir.

For computing distance, a P-wave velocity of 6040 m/s was used. This value was determined by averaging the sonic logs of wells 34-7 and 34-10 over the 3 porosity zones of the reservoir. The ratio of P-wave velocity to S-wave velocity was taken to be 1.75. This is a reasonable ratio for brine-saturated dolomites and anhydrites using the P-wave velocity above (Rafavich et al., 1984).

The data that were digitally acquired in the field were too under sampled to successfully apply the hodogram technique. Only the events that were digitized from analog tapes could be located. These data were edited based on the ellipticity of the hodograms. Events with the ratio of the major-to-minor axes of the ellipse trajectory less than 4.0 were eliminated for mapping purposes because the direction to the event was considered poorly constrained. The high-frequency noise

contaminating the data late in the experiment, mentioned above, restricted the detection of any mappable events after June 27. Seventy-three events were selected for mapping, all of which occurred on the nights of June 19 and 23 (Figure 2). None of the 4 events detected during the pressurized injection of June 7 had reliable hodograms. The first 2 ms of P-wave particle motion, about one-half of a cycle, were used in hodogram trajectory measurements. In a series of test, lengthening the first arrival data used increasingly aligned event trajectories 45° from the horizontal components. We suspect that a strong geophone site response caused the event trajectories to align at 45° from the two axes. The effect was minimized adequately by using only the first half-cycle of particle motion. All events were rotated to geographic coordinates by determining the location of the orientation shot via the hodogram technique. As with the event trajectories, a half-cycle (14 ms) of the shot first arrival was used. The trajectory ellipse passed our criteria of requiring a ratio of major-to-minor axes greater than 4.0, but the signal-to-noise ratio of the horizontal components was poor because shot energy, coming from the surface, had a steep vertical incidence. Therefore, the absolute orientation of seismicity is not reliably known.

Figure 5 shows the locations of events that occurred on the nights of June 19 and 23. The location map shows no distinct trends. However, if the events which occurred on the night of June 19 alone are mapped, two distinct, parallel trends striking NE-SW can be identified (Figure 6). Events were detected at distances up to 1700 m from monitor well 34-7, but most occurred within 900 m. There is a 180° ambiguity in locating events using only one downhole receiving station since its azimuth relative to the direction of shear motion at the microearthquake source is unknown. An observed first motion may be a compression first arrival from the indicated direction or a rarefaction first arrival from the opposite direction. We have arbitrarily plotted all events to the SW of monitor well 34-7. Some or all of the microearthquakes could have occurred to the NE of the monitor well. If the events were plotted on either side, the azimuthal trends of seismicity would not change. In a test, we assumed that all first motions were compressive, so that events plotted on each side of the monitor well. The orientation of the trends indicated in Figure 6 could be identified symmetrically about the monitor well. Since no events occurred close to the monitor well, allowing events to be located on both sides of the geophone results in the unlikely possibility of a gap in seismicity that is equally spaced on each side of the well. Thus, most events must have occurred to one side or the other of the geophone station, and, if so, the sense of shear motions, either left-lateral or right-lateral, are not consistent at the sources of microearthquakes which occurred along linear trends.

The microearthquake locations, as shown in Figure 5, occurred near producing wells and away from the injection wells 34-10 and 34-12. No events occurred within 140 m of wells 34-10 and 34-12. If all events are mapped to the northeast of the monitor well 34-7, the relationship of event locations with respect to the closest injection well, 34-2, are identical to that shown for injection well 34-10 in Figure 5. Despite the 180° ambiguity in event locations, it can be concluded that the microearthquakes, as best as can be mapped, occurred in the vicinities of producing wells and away from the injection wells.

DISCUSSION

Little seismicity was detected during the pressurized injection phase and most occurred during normal waterflood activity in the field. The model usually used to explain induced seismicity is Mohr-Coulomb failure in which effective rock strengths are reduced by increased pore pressure, and shear failure occurs when fluid pressure exceeds some critical level. With this model, seismicity would be expected to occur in high pressure areas close to the injection well as soon as pressure builds up over sufficiently large areas. The paucity of microearthquakes during the pressurized injection phase and the subsequent relative abundance of microearthquakes

occurring near producing wells, where pressures would be expected to be relatively low in the reservoir (Figure 5), suggest a mechanism other than Mohr-Coulomb failure is controlling induced seismicity. We suspect that microseismicity is being induced by the reduction of pore pressure in the reservoir. Other investigators have reported cases of earthquakes induced from the withdrawl of reservoir fluid (e.g. Davis and Pennington, 1989). There are various ways microseismicity could be induced by reduction in pore pressure. Laboratory experiments have shown that decreasing pore pressure can change the characteristics of movement along a fault from aseismic stable sliding to seismic stick-slip (Byerlee and Brace, 1972). If aseismic deformation is taking place in the reservoir due to tectonic or overburden stresses, the lowering of pore pressures could induce microearthquakes by changing the mode of deformation within the reservoir to seismic stick-slip. Withdrawl of reservoir fluids could also induce microearthquakes as a result of differential compaction along pre-existing fractures or faults in or above areas of the reservoir that are being depleted. Davis and Pennington (1989) have applied a failure model which incorporates stress loading, on larger time and spatial scales than our study, to explain earthquake occurrence in relatively low pressure areas of a waterflooded oil field of Texas.

A more thorough, long term experiment is needed to verify if indeed microearthquakes are occurring in low pressure areas of the reservoir and to more accurately monitor how microseismicity varies with production and flooding activity. Specifically, constant monitoring time capability at several downhole geophone stations (at least 3) is needed to produce an accurate microearthquake location map and to reliably characterize seismic recurrence in the field. Finally, modeling pressure variations in the field, using tracer data and individual well production-injection volumes, may explain the mechanism causing microearthquakes and thereby allow the prediction of microseismicity which will be useful in understanding fluid flow within the reservoir.

CONCLUSIONS

Microseismic monitoring of the Chaveroo oil field during a 3000-barrel pressurized injection of water over a 5.5-hour period resulted in little detectable seismicity. Intermittent monitoring over a 5-week period following the injection indicated detectable seismicity occurred during normal waterflood production. Monitoring during the 5 weeks, however, was not complete enough to draw general conclusions on the temporal variations of microseismicity observed.

Seventy-three good quality events recorded over a cumulative 24 hours of intermittent monitoring were located using the hodogram technique. Events were detected at distances up to 1700 m from the monitor well, but most occurred within 900 m. The map of microearthquake locations indicates that events occurred in the vicinity of producing wells and away from injection wells. The first half of the sequence of mappable events occurred along linear trends, but the pattern became more scattered during the later half of the sequence.

The lack of seismicity during the pressurized injection and the increased seismicity levels occurring away from injection wells during normal waterflooding, suggest seismicity is not induced by Mohr-Coulomb failure. We suspect, as proposed by previous investigators, that seismicity could be induced by the decrease of pore pressure resulting from reservoir fluid withdrawl.

ACKNOWLEDGMENT

The field experiment was a collaborative effort between Los Alamos National Laboratory and

the Murphy Operating Corporation (MOC) working under the auspices of the DOE's Oil Recovery Technology Partnership. We gratefully acknowledge Robert J. Hanold, co-Chairman of the Partnership, who encouraged us to undertake the project and contributed to its planning and execution.

REFERENCES

Aki, K,. and Richards, P. G., 1980, Quanitative seismology, theory and methods, volume 2: W. H. Freeman and Co.

Byerlee, J. D., and Brace, W. F., 1972, Fault stability and pore pressure: Bull. Seis. Soc. Am., **62**, 657-660.

Davis, S. D., and Pennington, W. D., 1989, Induced seismic deformation in the Cogdell oil field of west Texas: Bull. Seis. Soc. Am., **79**, 1477-1495.

Fehler, M., House, L., and Kaieda, H., 1987, Determining planes along which earthquakes occur: method and application to earthquakes accompanying hydraulic fracturing: J. Geophys. Res., **92**, 9407-9414.

Matsumura, S., 1981, Three-dimensional expression of seismic particle motions by the trajectory ellipsoid and its application to the seismic data observed in the Kanto District, Japan: J. Phys. Earth, **29**, 221-239.

Rafavich, F., Kendall, C. H. St. C., and Todd, T. P., 1984, The relationship between acoustic properties and the petrographic character of carbonate rocks: Geophysics **49**, 1622-1636.

FIGURE CAPTIONS

Fig. 1. General location map and the well configuration of Section 34 of the Murphy Operating Corporation's Haley Unit of the Chaveroo oil field, New Mexico.

Fig. 2. Number of microearthquakes detected from analog tape per 12 hour recording session.

Fig. 3. Number of microearthquakes detected by the field digital event recorder per 40 hour recording session.

Fig. 4. Three components of a typical microseismic event detected (above) and the displacement amplitude spectrum of the P- and S-wave of the horizontal component H1 (below).

Fig. 5. Microearthquake location map for events detected on June 19 and 23. I=injector well, M=monitor well

Fig. 6. Microearthquake location map for the events detected on June 19 shown with the interpreted trends. I=injector well, M=monitor well

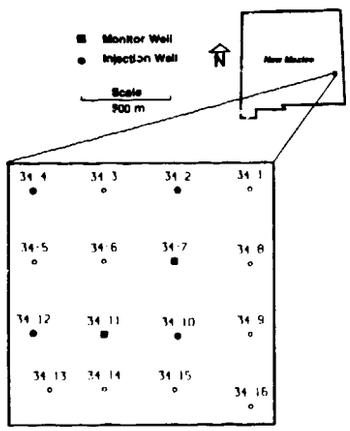

Fig. 1. General location map and the well configuration of Section 34 of the Murphy Operating Corporation's Haley Unit of the Chaveroo oil field, New Mexico.

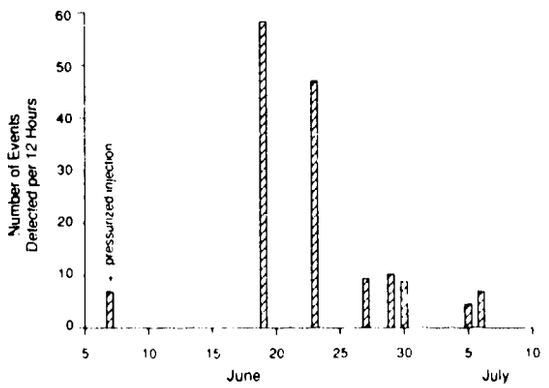

Fig. 2. Number of microearthquakes detected from analog tape per 12 hour recording session.

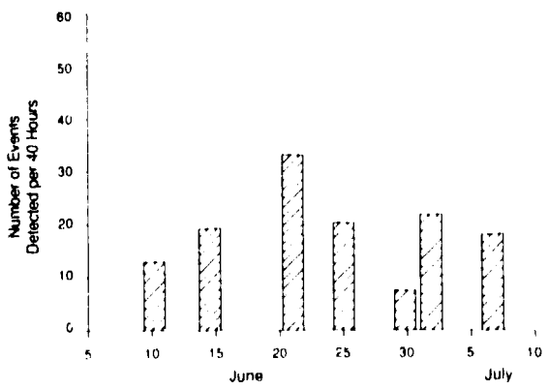

Fig. 3. Number of microearthquakes detected by the field digital event recorder per 40 hour recording session.

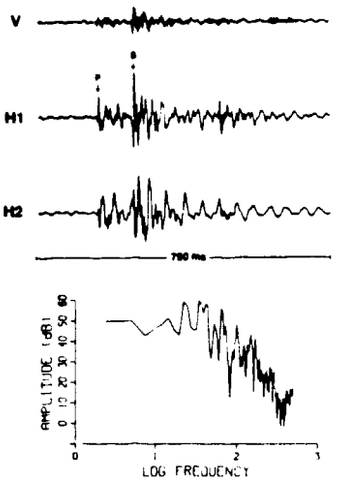

Fig. 4. Three components of a typical microseismic event detected (above) and the displacement amplitude spectrum of the P- and S-wave of the horizontal component H1 (below).

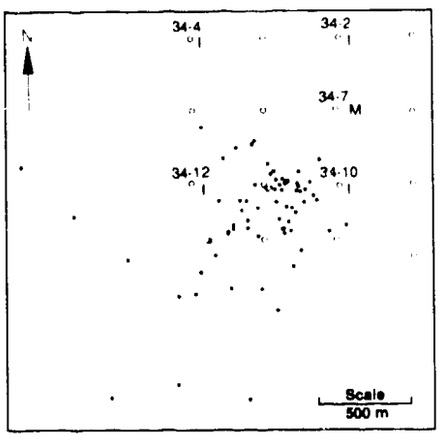

Fig. 5. Microearthquake location map for events detected on June 19 and 23. I=injector well, M=monitor well

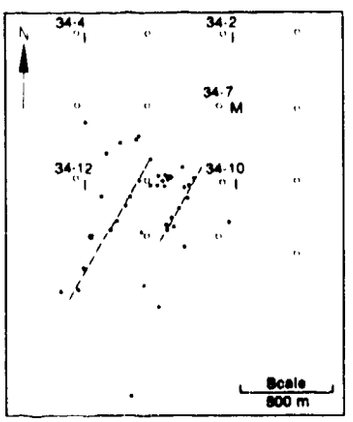

Fig. 6. Microearthquake location map for the events detected on June 19 shown with the interpreted trends. I=injector well, M=monitor well